ISSN 1674-1056
http://cpb.iphy.ac.cn
http://iopscience.iop.org/cpb
中国物理 B
Chinese Physics
中国物理 Chinese Physics B

Improved reproducing kernel particle method for piezoelectric materials

Ji-Chao Ma(马吉超), Gao-Feng Wei(魏高峰), Dan-Dan Liu(刘丹丹)
Citation: Chin. Phys. B . 2018, 27(1): 010201. **doi:** 10.1088/1674-1056/27/1/010201

Journal homepage: http://cpb.iphy.ac.cn; http://iopscience.iop.org/cpb

What follows is a list of articles you may be interested in

Two-dimensional fracture analysis of piezoelectric material based on the scaled boundary node method

Shen-Shen Chen(陈莘莘), Juan Wang(王娟), Qing-Hua Li(李庆华)
Chin. Phys. B . 2016, 25(4): 040203. **doi:** 10.1088/1674-1056/25/4/040203

An interpolating reproducing kernel particle method for two-dimensional scatter points

Qin Yi-Xiao, Liu Ying-Ying, Li Zhong-Hua, Yang Ming
Chin. Phys. B . 2014, 23(7): 070207. **doi:** 10.1088/1674-1056/23/7/070207

Analysis of variable coefficient advection–diffusion problems via complex variable reproducing kernel particle method

Weng Yun-Jie, Cheng Yu-Min
Chin. Phys. B . 2013, 22(9): 090204. **doi:** 10.1088/1674-1056/22/9/090204

Combine complex variable reproducing kernel particle method and finite element method for solving transient heat conduction problems

Chen Li, Ma He-Ping, Cheng Yu-Min
Chin. Phys. B . 2013, 22(5): 050202. **doi:** 10.1088/1674-1056/22/5/050202

Improved reproducing kernel particle method for piezoelectric materials*

Ji-Chao Ma(马吉超)[1], Gao-Feng Wei(魏高峰)[1,†], and Dan-Dan Liu(刘丹丹)[2]

[1] School of Mechanical and Automotive Engineering, Qilu University of Technology, Jinan 250353, China
[2] College of Foreign Languages, Shandong Normal University, Jinan 250014, China

(Received 2 August 2017; revised manuscript received 15 September 2017; published online 28 November 2017)

In this paper, the normal derivative of the radial basis function (RBF) is introduced into the reproducing kernel particle method (RKPM), and the improved reproducing kernel particle method (IRKPM) is proposed. The method can decrease the errors on the boundary and improve the accuracy and stability of the algorithm. The proposed method is applied to the numerical simulation of piezoelectric materials and the corresponding governing equations are derived. The numerical results show that the IRKPM is more stable and accurate than the RKPM.

Keywords: meshless methods, piezoelectric materials, reproducing kernel particle method, radial basis function method

PACS: 02.30.Jr, 02.60.–x, 02.60.Cb, 02.60.Lj **DOI:** 10.1088/1674-1056/27/1/010201

1. Introduction

Numerical simulation has become the main method to research the material mechanical property, because it can quickly and efficiently solve the problem domain. Numerical simulation methods mainly include the finite element method (FEM),[1] boundary element method, and meshless method.[2–4] When FEM is used to accurately solve the local domain, the mesh refinement is heavy, which results in costing a lot of computing time. The boundary element method might produce strong singularity near the singular point, which makes the problem difficult to calculate. The meshless method has the advantages of quick calculation and high precision when it is used to solve the local domain. So it has been developed in recent years.

The difference between the meshless method and FEM is that the meshless method uses the nodes to approximate the problem domain and its boundary instead of meshes. It does not require strict element connectivity data, and is not subject to much degradation in accuracy when nodal arrangements are very irregular. When the local problem domain needs to be solved accurately, it only needs to increase the number of nodes. The work is less than FEM. Therefore, the computation time and the amount of storage can be saved.

There are a variety of meshless methods, such as the reproducing kernel particle method (RKPM),[5–8] discontinuous Galerkin method (DGM),[9] polynomial point interpolation method (PPIM),[10,11] boundary integral equation method (BIEM),[12,13] element-free Galerkin method (EFGM),[14–17] moving least-squares method (MLSM),[18–20] smooth particle hydrodynamics (SPH),[21,22] iterative Galerkin method (IGM),[23] radial basis function method (RBFM),[24,25] the partition of unity method (PUM),[26,27] meshless local Petrov–Galerkin method (MLPG),[28–31] finite point method (FPM),[32,33] Hermite-type radial point interpolation method (Hermite-type RPIM),[34–36] meshless manifold method (MMM),[37,38] and complex variable meshless method (CVMM).[39,40]

The SPH method, which is based on the kernel estimate introduced by Monaghan, is the earliest meshless method. When dealing with finite field problems, the SPH method leads to low computational accuracy and unstability. To overcome the disadvantages of the SPH method, Liu proposed the RKPM by introducing a corrected function to integral transform.[41] The RKPM not only improves the computational accuracy but also enhances the stability. But the RKPM has a great computational cost owing to a great number of nodes selected in the domain. To overcome the disadvantage, Chen proposed the complex variables reproducing kernel particle method (CVRKPM).[8] The advantage of CVRKPM is that once the shape function is obtained, the correction function of a two-dimensional problem is formed with a one-dimensional basis function. The Ohs combined reproducing kernel function with the collocation method to propose the meshless point collocation method, by which the piezoelectric device was analyzed.[4]

The RKPM has a fast convergence speed and high accuracy, so it is mainly used to solve displacements and electric potential of piezoelectric materials.[42,43] But in the process of

*Project supported by the National Natural Science Foundation of China (Grant No. 11271234) and the Shandong Provincial Science Foundation, China (Grant No. ZR2017MA028).

†Corresponding author. E-mail: wgf@spu.edu.cn

© 2018 Chinese Physical Society and IOP Publishing Ltd

solving the domain, the computational accuracy of the nodes at the boundary cannot meet the requirements. In this paper, the improved reproducing kernel particle method (IRKPM) is proposed to improve the RKPM, which adds the normal derivative of the radial basis function (RBF). In the process of solving the approximate function, the kernel function of the RKPM is constructed by all nodes in the domain, and the normal derivatives of the RBFs are constructed by nodes on the boundary. The method can decrease the error on the boundary. The accuracy and stability of the proposed method are demonstrated by the numerical examples.

2. The approximate displacement function constructed by IRKPM

In the z-direction, the approximate displacement function $w^h(x,z)$ can be expressed as the linear combination of RKPMs (constructed by n_m nodes) and $n_{\rm DB}$ normal derivative of RBFs in local supporting domain

$$w^h(x,z)=\sum_{k=1}^{n_m}R_k^m(x,z)c_k+\sum_{j=1}^{n_{\rm DB}}\frac{\partial R_j^{\rm DB}(x,z)}{\partial n}b_j, \tag{1}$$

where b_j and c_k are undetermined coefficients, n_m is the number of nodes in the local supporting domain, and $n_{\rm DB}$ is the number of nodes on the boundary.

The term of RKPM is

$$R_k^m(x,z)=c_k^m(x-x_I,z-z_I)w(r_I)R_k^m(x_I,z_I)\Delta V_I, \tag{2}$$

where x_I and z_I are coordinates of node I, $R_k^m(x_I,z_I)$ is the unknown nodal parameter at node I, ΔV_I is a measure of domain surrounding node I, and

$$c_k^m(x-x_I,z-z_I)=\boldsymbol{b}_k^{\rm T}(x,z)\boldsymbol{p}_k(x-x_I,z-z_I), \tag{3}$$

with coefficient matrix

$$\boldsymbol{b}_k(x,z)=[b_1(x,z)\quad b_2(x,z)\quad\cdots\quad b_6(x,z)]^{\rm T}, \tag{4}$$

which can be obtained by the reproducing conditions of kernel approximation.

For a two-dimensional problem, the polynomial basis function vector $\boldsymbol{p}_k$ can be expressed as a quadratic basis function

$$\begin{aligned}&\boldsymbol{p}_k^{\rm T}(x-x_I,z-z_I)\\&=[1,x-x_I,z-z_I,(x-x_I)^2,(x-x_I)(z-z_I),(z-z_I)^2].\end{aligned} \tag{5}$$

In Eq. (2), $r_I=d_I/d_{mI}$, $d_I=\sqrt{(x-x_I)^2+(z-z_I)^2}$, d_{mI} is the radius of the supporting domain at node (x_I,z_I), and

$$w(r_I)=\begin{cases}2/3-4r_I^2+4r_I^3, & r_I\le 1/2,\\ 4/3-4r_I+4r_I^2-4r_I^3/3, & 1/2<r_I\le 1,\\ 0, & r_I>1.\end{cases} \tag{6}$$

In Eq. (1), $R_j^{\rm DB}(x,z)$ is a class of function whose values depend only on the distance between evaluation nodes (x,z) and the nodes (x_j,z_j), $r_j=\sqrt{(x-x_j)^2+(z-z_j)^2}$, as

$$\begin{aligned}R_j^{\rm DB}(x,z)&=\left(1-\frac{r_j}{\delta}\right)^5\left(8+40\frac{r_j}{\delta}+48\frac{r_j^2}{\delta^2}\right.\\&\quad\left.+25\frac{r_j^3}{\delta^3}+5\frac{r_j^4}{\delta^4}\right),\end{aligned} \tag{7}$$

$$\frac{\partial R_j^{\rm DB}(x,z)}{\partial n}=l_{xj}\frac{\partial R_j^{\rm DB}(x,z)}{\partial x}+l_{zj}\frac{\partial R_j^{\rm DB}(x,z)}{\partial z}, \tag{8}$$

where δ is the shaped parameter, $l_{xj}=\cos(n,x_j)$, and $l_{zj}=\cos(n,z_j)$ is the direction cosine.

Equation (1) can be rewritten into the matrix form

$$w^h(x,z)=\boldsymbol{B}^{\rm T}\boldsymbol{a}_0, \tag{9}$$

where $\boldsymbol{B}$ is the basis function vector

$$\boldsymbol{B}^{\rm T}=\left[R_1^k(x,z)\quad\cdots\quad R_{n_m}^k(x,z)\quad\frac{\partial R_1^{\rm DB}}{\partial n}\quad\cdots\quad\frac{\partial R_{n_{\rm DB}}^{\rm DB}}{\partial n}\right], \tag{10}$$

and the coefficient vector $\boldsymbol{a}_0$ is

$$\boldsymbol{a}_0^{\rm T}=[c_1\ \ c_2\ \ \cdots\ \ c_{n_m}\ \ b_1\ \ b_2\ \ \cdots\ \ b_{n_{\rm DB}}]. \tag{11}$$

In Eq. (1), coefficients c_k and b_j can be confirmed by n_m nodes values in the supporting domain and the derivative values of $n_{\rm DB}$ nodes on the boundary.

$w(x_l,z_l)$ can be obtained as

$$w(x_l,z_l)=\sum_{k=1}^{n_m}R_k^m(x_l,z_l)c_k+\sum_{j=1}^{n_{\rm DB}}\frac{\partial R_j^{\rm DB}(x_l,z_l)}{\partial n}b_j, \tag{12}$$

where $l=1,2,\ldots,n_m$.

The following constraint is applied to get the unique solution:

$$\sum_{k=1}^{n_m}\frac{\partial R_j^{\rm DB}(x_k,z_k)}{\partial n}c_k=0, \tag{13}$$

where $j=1,2,\ldots,n_{\rm DB}$.

Simultaneously considering Eqs. (12) and (13), the matrix equation can be expressed as

$$\boldsymbol{W}_s=\begin{Bmatrix}w(x_l,z_l)\\0\end{Bmatrix}=\begin{Bmatrix}\boldsymbol{R}_0 & \boldsymbol{R}_1\\ \boldsymbol{R}_1^{\rm T} & 0\end{Bmatrix}\begin{Bmatrix}\boldsymbol{c}\\ \boldsymbol{b}\end{Bmatrix}=\boldsymbol{G}\boldsymbol{a}_0, \tag{14}$$

where $\boldsymbol{G}$ is the generalized torque matrix.

The torque matrix of RKPMs can be structured by n_m nodes

$$\boldsymbol{R}_0 = \begin{bmatrix} R_1^m(x_1,z_1) & R_2^m(x_1,z_1) & \cdots & R_{n_m}^m(x_1,z_1) \\ R_1^m(x_2,z_2) & R_2^m(x_2,z_2) & \cdots & R_{n_m}^m(x_2,z_2) \\ \vdots & \vdots & \ddots & \vdots \\ R_1^m(x_{n_m},z_{n_m}) & R_2^m(x_{n_m},z_{n_m}) & \cdots & R_{n_m}^m(x_{n_m},z_{n_m}) \end{bmatrix}_{(n_m\times n_m)}. \tag{15}$$

The first-order derivative value of the torque matrix for the RBFs in n_{DB} nodes is

$$\boldsymbol{R}_1 = \begin{bmatrix} \dfrac{\partial R_1^{\mathrm{DB}}(x_1,z_1)}{\partial n} & \dfrac{\partial R_2^{\mathrm{DB}}(x_1,z_1)}{\partial n} & \cdots & \dfrac{\partial R_{n_{\mathrm{DB}}}^{\mathrm{DB}}(x_1,z_1)}{\partial n} \\ \dfrac{\partial R_1^{\mathrm{DB}}(x_2,z_2)}{\partial n} & \dfrac{\partial R_2^{\mathrm{DB}}(x_2,z_2)}{\partial n} & \cdots & \dfrac{\partial R_{n_{\mathrm{DB}}}^{\mathrm{DB}}(x_2,z_2)}{\partial n} \\ \vdots & \vdots & \ddots & \vdots \\ \dfrac{\partial R_1^{\mathrm{DB}}(x_{n_m},z_{n_m})}{\partial n} & \dfrac{\partial R_2^{\mathrm{DB}}(x_{n_m},z_{n_m})}{\partial n} & \cdots & \dfrac{\partial R_{n_{\mathrm{DB}}}^{\mathrm{DB}}(x_{n_m},z_{n_m})}{\partial n} \end{bmatrix}_{(n_m\times n_{\mathrm{DB}})}. \tag{16}$$

Because the generalized torque matrix $\boldsymbol{G}$ is a symmetrical matrix, the coefficient vector $\boldsymbol{a}_0$ can be obtained by solving Eq. (14)

$$\boldsymbol{a}_0 = \boldsymbol{G}^{-1}\boldsymbol{W}_s. \tag{17}$$

Substituting Eq. (17) into Eq. (9), the relation can be obtained as

$$w^h(x,z) = \boldsymbol{B}^{\mathrm{T}}\boldsymbol{a}_0 = \boldsymbol{B}^{\mathrm{T}}\boldsymbol{G}^{-1}\boldsymbol{W}_s = \boldsymbol{\Phi}^{\mathrm{T}}\boldsymbol{W}_s, \tag{18}$$

$$\boldsymbol{\Phi}^{\mathrm{T}} = \boldsymbol{B}^{\mathrm{T}}\boldsymbol{G}^{-1} = \begin{bmatrix}\phi_1 & \phi_2 & \cdots & \phi_{n_m} & \phi_1^H & \cdots & \phi_{n_{\mathrm{DB}}}^H\end{bmatrix}_{1\times(n_m+n_{\mathrm{DB}})}, \tag{19}$$

where $\boldsymbol{\Phi}$ is the shaped function vector.

Substituting Eq. (19) into Eq. (18), the approximate function can be found as

$$w^h(x,z) = \boldsymbol{\Phi}^{\mathrm{T}}\boldsymbol{W}_s = \sum_{i=1}^{n_m}\phi_i w_i = \begin{bmatrix}\phi_1 & \phi_2 & \cdots & \phi_{n_m}\end{bmatrix}\begin{bmatrix} w_1 \\ w_2 \\ \vdots \\ w_{n_m}\end{bmatrix} = \boldsymbol{N}\hat{\boldsymbol{w}}, \tag{20}$$

and

$$w^h(x,z)_{,x} = \boldsymbol{N}_{,x}\hat{\boldsymbol{w}}, \tag{21}$$

$$w^h(x,z)_{,z} = \boldsymbol{N}_{,z}\hat{\boldsymbol{w}}, \tag{22}$$

$$w^h(x,z)_{,xx} = \boldsymbol{N}_{,xx}\hat{\boldsymbol{w}}, \tag{23}$$

$$w^h(x,z)_{,zz} = \boldsymbol{N}_{,zz}\hat{\boldsymbol{w}}, \tag{24}$$

$$w^h(x,z)_{,xz} = \boldsymbol{N}_{,xz}\hat{\boldsymbol{w}}, \tag{25}$$

where $\boldsymbol{N}_{,x}$, $\boldsymbol{N}_{,z}$, $\boldsymbol{N}_{,xx}$, $\boldsymbol{N}_{,zz}$, and $\boldsymbol{N}_{,xz}$ are the matrices containing the x, z, second x, second z, and x–z derivatives of the approximate function, respectively.

3. The governing equations of piezoelectric material

In the x–z plane, the constitutive equations of piezoelectric material can be expressed as

$$\sigma_p = c_{pq}^{\mathrm{E}}\varepsilon_q - e_{pk}E_k, \tag{26}$$

$$D_i = e_{iq}\varepsilon_q + \xi_{ik}^{\varepsilon}E_k, \tag{27}$$

where σ, ε, E_k, and D_i are the stress tensor, the strain tensor, the electric field vector, and the electric displacement vector, respectively. c^{E}, e, and ξ^{ε} are the elastic stiffness, piezoelectric constant, and dielectric constant, respectively. Superscript ε and E represent coefficients measured at constant strain and electric field, respectively.

The relation between strain and displacement is

$$\varepsilon_{ij} = \frac{1}{2}(u_{i,j} + u_{j,i}). \tag{28}$$

The above condensed matrix can be rewritten as

$$\varepsilon_x = \varepsilon_{xx} = u_{,x}, \tag{29}$$

$$\varepsilon_z = \varepsilon_{zz} = w_{,z}, \tag{30}$$

$$\gamma_{xz} = 2\varepsilon_{xz} = u_{,z} + w_{,x}, \tag{31}$$

where u and w represent the displacement functions in the x and z directions, respectively. Commas followed by indices represent partial differentiation with respect to that index.

The relationship between electric field and electric potential is

$$E_i = -\varphi_{,i}. \tag{32}$$

The mechanical constitutive equation of piezoelectric material is expressed as the two-dimensional matrix form

$$\begin{bmatrix}\sigma_x \\ \sigma_z \\ \tau_{xz}\end{bmatrix} = \begin{bmatrix} c_{11} & c_{13} & 0 \\ c_{13} & c_{33} & 0 \\ 0 & 0 & c_{55}\end{bmatrix}\begin{bmatrix}\varepsilon_x \\ \varepsilon_z \\ \gamma_{xz}\end{bmatrix} - \begin{bmatrix} 0 & e_{31} \\ 0 & e_{33} \\ e_{15} & 0\end{bmatrix}\begin{bmatrix}E_x \\ E_z\end{bmatrix}. \tag{33}$$

The two-dimensional matrix form of the electrostatic constitutive equation is

$$\begin{bmatrix} D_x \\ D_z \end{bmatrix} = \begin{bmatrix} 0 & 0 & e_{15} \\ e_{31} & e_{33} & 0 \end{bmatrix} \begin{bmatrix} \varepsilon_x \\ \varepsilon_z \\ \gamma_{xz} \end{bmatrix} + \begin{bmatrix} \xi_{11}^{\varepsilon} & 0 \\ 0 & \xi_{33}^{\varepsilon} \end{bmatrix} \begin{bmatrix} E_x \\ E_z \end{bmatrix}. \quad (34)$$

The mechanical and electrostatic constitutive equations can be rewritten as

$$\begin{bmatrix} \varepsilon_x \\ \varepsilon_z \\ \gamma_{xz} \end{bmatrix} = \begin{bmatrix} s_{11} & s_{13} & 0 \\ s_{13} & s_{33} & 0 \\ 0 & 0 & s_{55} \end{bmatrix} \begin{bmatrix} \sigma_x \\ \sigma_z \\ \tau_{xz} \end{bmatrix} + \begin{bmatrix} 0 & d_{31} \\ 0 & d_{33} \\ d_{15} & 0 \end{bmatrix} \begin{bmatrix} E_x \\ E_z \end{bmatrix}, \quad (35)$$

$$\begin{bmatrix} D_x \\ D_z \end{bmatrix} = \begin{bmatrix} 0 & 0 & d_{15} \\ d_{31} & d_{33} & 0 \end{bmatrix} \begin{bmatrix} \sigma_x \\ \sigma_z \\ \tau_{xz} \end{bmatrix} + \begin{bmatrix} \xi_{11}^{\sigma} & 0 \\ 0 & \xi_{33}^{\sigma} \end{bmatrix} \begin{bmatrix} E_x \\ E_z \end{bmatrix}, \quad (36)$$

where d_{ij} is the piezoelectric constant, s_{ij} is the elastic compliance constant, and ξ_{ij}^{σ} is the dielectric constant. The superscript σ represents quantities measured at constant stress.

In the x–z plane, the governing mechanical equilibrium equation is

$$\sigma_{ij,j} = 0. \quad (37)$$

The electrostatic equilibrium equation is

$$D_{i,i} = 0. \quad (38)$$

Substituting Eqs. (26), (27), and (29)–(32) into Eqs. (37) and (38), the equilibrium equations can be rewritten. The governing mechanical equilibrium equations are

$$c_{11}u_{,xx} + c_{55}u_{,zz} + (c_{13}+c_{55})w_{,xz} + (e_{31}+e_{15})\varphi_{,xz} = 0, \quad (39)$$

$$(c_{13}+c_{55})u_{,xz} + c_{33}w_{,zz} + c_{55}w_{,xx} + e_{33}\varphi_{,zz} + e_{15}\varphi_{,xx} = 0. \quad (40)$$

The governing electrostatic equilibrium equation is

$$(e_{31}+e_{15})u_{,xz} + e_{15}w_{,xx} + e_{33}w_{,zz} - \xi_{11}^{\varepsilon}\varphi_{,xx} - \xi_{33}^{\varepsilon}\varphi_{,zz} = 0. \quad (41)$$

4. The governing equation of piezoelectric material

Once the approximation function is established, the next step is to discretize the partial differential equations. In this paper, the collocation method is used to discretize the governing equations. In the two-dimensional plane, piezoelectric material has three unknown values associated with every node in the domain, which are the displacement in the x-direction, the displacement in the z-direction, and the electric potential. The collocation method forces the unknown values of each node to satisfy the governing equations or the corresponding boundary conditions.

The mechanical governing equations are discretized into

$$c_{11}\boldsymbol{N}_{,xx}\hat{\boldsymbol{u}} + c_{55}\boldsymbol{N}_{,zz}\hat{\boldsymbol{u}} + (c_{13}+c_{55})\boldsymbol{N}_{,xz}\hat{\boldsymbol{w}} + (e_{31}+e_{15})\boldsymbol{N}_{,xz}\hat{\boldsymbol{\varphi}} = 0, \quad (42)$$

$$(c_{13}+c_{55})\boldsymbol{N}_{,xz}\hat{\boldsymbol{u}} + c_{33}\boldsymbol{N}_{,zz}\hat{\boldsymbol{w}} + c_{55}\boldsymbol{N}_{,xx}\hat{\boldsymbol{w}} + e_{33}\boldsymbol{N}_{,zz}\hat{\boldsymbol{\varphi}} + e_{15}\boldsymbol{N}_{,xx}\hat{\boldsymbol{\varphi}} = 0. \quad (43)$$

The electrostatic governing equation is discretized into

$$(e_{31}+e_{15})\boldsymbol{N}_{,xz}\hat{\boldsymbol{u}} + e_{15}\boldsymbol{N}_{,xx}\hat{\boldsymbol{w}} + e_{33}\boldsymbol{N}_{,zz}\hat{\boldsymbol{w}} - \xi_{11}^{\varepsilon}\boldsymbol{N}_{,xx}\hat{\boldsymbol{\varphi}} - \xi_{33}^{\varepsilon}\boldsymbol{N}_{,zz}\hat{\boldsymbol{\varphi}} = 0. \quad (44)$$

The unknown values of the nodes on the boundary are constructed to satisfy the corresponding boundary condition equations by the approximate function.

The mechanical boundary conditions for any node are given as

$$\sigma_x = 0 \Rightarrow c_{11}\boldsymbol{N}_{,x}\hat{\boldsymbol{u}} + c_{13}\boldsymbol{N}_{,z}\hat{\boldsymbol{w}} + e_{31}\boldsymbol{N}_{,z}\hat{\boldsymbol{\varphi}} = 0, \quad (45)$$

$$\sigma_z = 0 \Rightarrow c_{13}\boldsymbol{N}_{,x}\hat{\boldsymbol{u}} + c_{33}\boldsymbol{N}_{,z}\hat{\boldsymbol{w}} + e_{33}\boldsymbol{N}_{,z}\hat{\boldsymbol{\varphi}} = 0, \quad (46)$$

$$\tau_{xz} = 0 \Rightarrow c_{55}\boldsymbol{N}_{,z}\hat{\boldsymbol{u}} + c_{55}\boldsymbol{N}_{,x}\hat{\boldsymbol{w}} + e_{15}\boldsymbol{N}_{,x}\hat{\boldsymbol{\varphi}} = 0, \quad (47)$$

$$u = 0 \Rightarrow \boldsymbol{N}\hat{\boldsymbol{u}} = 0, \quad (48)$$

$$w = 0 \Rightarrow \boldsymbol{N}\hat{\boldsymbol{w}} = 0. \quad (49)$$

Similarly, the electrostatic boundary conditions for nodes are

$$\varphi_{,x} = 0 \Rightarrow \boldsymbol{N}_{,x}\hat{\boldsymbol{\varphi}} = 0, \quad (50)$$

$$\varphi = V \Rightarrow \boldsymbol{N}\hat{\boldsymbol{\varphi}} = V. \quad (51)$$

Finally, the governing equation can be expressed as the matrix form by the IRKPM

$$\begin{bmatrix} \boldsymbol{K}_{uu} & \boldsymbol{K}_{uw} & \boldsymbol{K}_{u\varphi} \\ \boldsymbol{K}_{wu} & \boldsymbol{K}_{ww} & \boldsymbol{K}_{w\varphi} \\ \boldsymbol{K}_{\varphi u} & \boldsymbol{K}_{\varphi w} & \boldsymbol{K}_{\varphi\varphi} \end{bmatrix} \begin{bmatrix} \hat{\boldsymbol{u}} \\ \hat{\boldsymbol{w}} \\ \hat{\boldsymbol{\varphi}} \end{bmatrix} = \begin{bmatrix} \boldsymbol{F}_u \\ \boldsymbol{F}_w \\ \boldsymbol{F}_{\varphi} \end{bmatrix}. \quad (52)$$

In the x-direction, the mechanical equilibrium equations are

$$\boldsymbol{K}_{uu} = c_{11}\boldsymbol{N}_{,xx} + c_{55}\boldsymbol{N}_{,zz}, \quad (53)$$

$$\boldsymbol{K}_{uw} = (c_{13}+c_{55})\boldsymbol{N}_{,xz}, \quad (54)$$

$$\boldsymbol{K}_{u\varphi} = (e_{31}+e_{15})\boldsymbol{N}_{,xz}, \quad (55)$$

$$\boldsymbol{F}_u = 0. \quad (56)$$

In the z-direction, the mechanical equilibrium equations are

$$\boldsymbol{K}_{wu} = (c_{13}+c_{55})\boldsymbol{N}_{,xz}, \quad (57)$$

$$\boldsymbol{K}_{ww} = c_{33}\boldsymbol{N}_{,zz} + c_{55}\boldsymbol{N}_{,xx}, \quad (58)$$

$$\boldsymbol{K}_{w\varphi} = e_{33}\boldsymbol{N}_{,zz} + e_{15}\boldsymbol{N}_{,xx}, \quad (59)$$

$$\boldsymbol{F}_w = 0. \quad (60)$$

The electrostatic equilibrium equations are

$$\boldsymbol{K}_{\varphi u} = (e_{33}+e_{15})\boldsymbol{N}_{,xz}, \quad (61)$$

$$\boldsymbol{K}_{\varphi w} = e_{15}\boldsymbol{N}_{,xx} + e_{33}\boldsymbol{N}_{,zz}, \quad (62)$$

$$\boldsymbol{K}_{\varphi\varphi} = -\xi_{11}^{\varepsilon}\boldsymbol{N}_{,xx} - \xi_{33}^{\varepsilon}\boldsymbol{N}_{,zz}, \quad (63)$$

$$\boldsymbol{F}_{\varphi} = 0. \quad (64)$$

5. Numerical examples

5.1. The piezoelectric strip

Take a 1.0×1.0 mm ($L = 1.0$ mm, $2h = 1.0$ mm) piezoelectric strip as the example to analyze the bending deformation, polarized in the z-direction. The strip is subjected to a linear stress in the x-direction and an applied voltage in the z-direction (shown in Fig. 1). The properties of the piezoelectric strip and other values are summarized in Table 1.

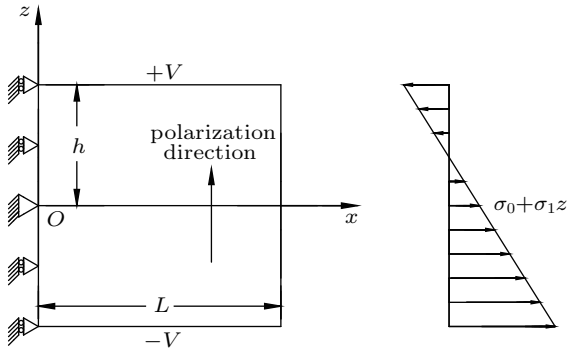


Fig. 1. The piezoelectric strip subjected to a linear stress and the voltage.

Table 1. Material properties, dimensions, and other constants.

s_{11}	1.64×10^{-5} mm^2/N	d_{31}	-1.72×10^{-7} mm/V
s_{13}	-7.22×10^{-6} mm^2/N	d_{33}	3.74×10^{-7} mm/V
σ_0	10 N/mm^2	ξ_{33}^{σ}	1.505×10^{-7} N/V^2
σ_1	-50 N/mm^3	V	1500 V
L	1.0 mm	h	0.5 mm

The mechanical and electrostatic boundary conditions are

$$\phi(x, z = \pm h) = \pm \mathrm{V}, \quad \sigma_z(x, z = \pm h) = 0, \quad \tau_{xz}(x, z = \pm h) = 0,$$
$$\phi_{,x}(x = L, z) = 0, \quad \sigma_x(x = L, z) = \sigma_0 + \sigma_1 z, \quad \tau_{xz}(x = L, z) = 0,$$
$$\phi_{,x}(x = 0, z) = 0, \quad u(x = 0, z) = 0, \quad w(x = 0, z = 0) = 0.$$

There are two factors to lead to the bending deformation of the piezoelectric strip. (i) The electric field is the same direction as the polarization, causing the piezoelectric strip to extend along the x-direction and contract in the z-direction. (ii) The piezoelectric strip bends upwards when a linear stress is applied. The deformation of the piezoelectric strip is the result of the electric field, magnetic field, and a linearly stress.

The comparisons of the nodal displacements are shown in Figs. 2 and 3, and the relative errors are analyzed in Fig. 4.

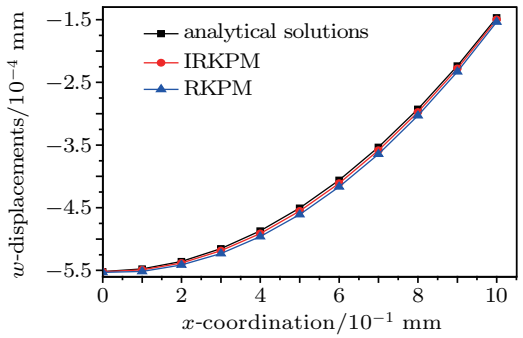


Fig. 2. (color online) Comparison of nodal displacements at $z = 0.5$.

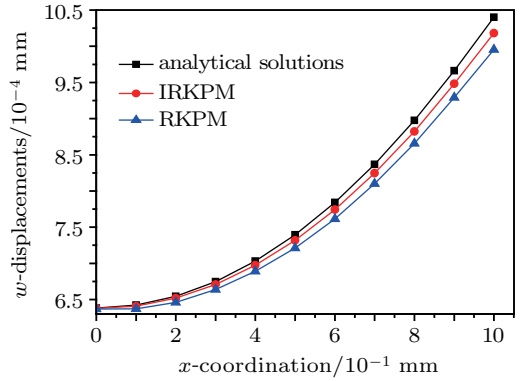


Fig. 3. (color online) Comparison of nodal displacements at $z = -0.5$.

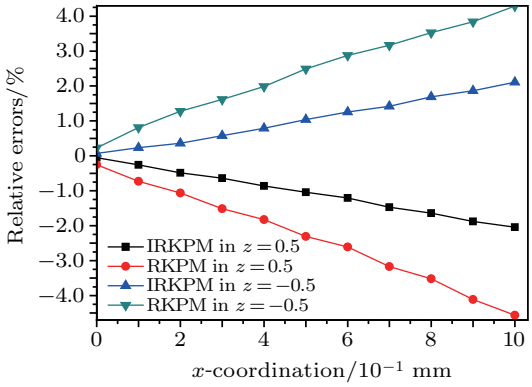


Fig. 4. (color online) Comparison of the relative errors for the IRKPM and the RKPM.

The nodal displacements and relative errors are calculated and listed in Tables 2 and 3.

Table 2. The nodal displacements and relative errors at $z = 0.5$.

Coordination	Analytical solution/mm	IRKPM displacement/mm	Relative error/%	RKPM displacement/mm	Relative error/%
(0, 0.5)	-5.518×10^{-4}	-5.521×10^{-4}	−0.05%	-5.532×10^{-4}	−0.25%
(1, 0.5)	-5.477×10^{-4}	-5.491×10^{-4}	−0.26%	-5.517×10^{-4}	−0.73%
(2, 0.5)	-5.356×10^{-4}	-5.382×10^{-4}	−0.49%	-5.413×10^{-4}	−1.06%
(3, 0.5)	-5.153×10^{-4}	-5.186×10^{-4}	−0.64%	-5.231×10^{-4}	−1.51%
(4, 0.5)	-4.870×10^{-4}	-4.912×10^{-4}	−0.86%	-4.959×10^{-4}	−1.83%
(5, 0.5)	-4.505×10^{-4}	-4.552×10^{-4}	−1.04%	-4.609×10^{-4}	−2.31%
(6, 0.5)	-4.060×10^{-4}	-4.109×10^{-4}	−1.21%	-4.166×10^{-4}	−2.61%
(7, 0.5)	-3.533×10^{-4}	-3.585×10^{-4}	−1.47%	-3.645×10^{-4}	−3.17%
(8, 0.5)	-2.926×10^{-4}	-2.974×10^{-4}	−1.64%	-3.029×10^{-4}	−3.52%
(9, 0.5)	-2.237×10^{-4}	-2.279×10^{-4}	−1.88%	-2.329×10^{-4}	−4.11%
(10, 0.5)	-1.468×10^{-4}	-1.498×10^{-4}	−2.04%	-1.535×10^{-4}	−4.56%

Table 3. The nodal displacements and relative errors $z = -0.5$.

Coordination	Analytical solution/mm	IRKPM displacement/mm	Relative error/%	RKPM displacement/mm	Relative error/%
(0, –0.5)	6.3825×10^{-4}	6.3780×10^{-4}	0.07%	6.368×10^{-4}	0.23%
(1, –0.5)	6.4230×10^{-4}	6.4080×10^{-4}	0.23%	6.371×10^{-4}	0.81%
(2, –0.5)	6.5445×10^{-4}	6.5210×10^{-4}	0.36%	6.461×10^{-4}	1.28%
(3, –0.5)	6.7470×10^{-4}	6.7080×10^{-4}	0.58%	6.638×10^{-4}	1.62%
(4, –0.5)	7.0305×10^{-4}	6.9750×10^{-4}	0.79%	6.891×10^{-4}	1.98%
(5, –0.5)	7.3950×10^{-4}	7.3180×10^{-4}	1.04%	7.211×10^{-4}	2.49%
(6, –0.5)	7.8405×10^{-4}	7.7420×10^{-4}	1.26%	7.615×10^{-4}	2.88%
(7, –0.5)	8.3670×10^{-4}	8.2480×10^{-4}	1.42%	8.102×10^{-4}	3.17%
(8, –0.5)	8.9745×10^{-4}	8.8230×10^{-4}	1.69%	8.658×10^{-4}	3.53%
(9, –0.5)	9.6630×10^{-4}	9.4830×10^{-4}	1.86%	9.292×10^{-4}	3.84%
(10, –0.5)	1.0400×10^{-3}	1.0181×10^{-3}	2.11%	9.954×10^{-4}	4.29%

From Table 2, it can be found that the maximum relative error between the IRKPM and the analytical solution is -2.04%, and the maximum relative error between the RKPM and the analytical solution is -4.56% in $z = 0.5$.

From Table 3, it can be found that the maximum relative error between the IRKPM and the analytical solution is 2.11%, and the maximum relative error between the RKPM and the analytical solution is 4.29% in $z = -0.5$.

The results obtained by the IRKPM are consistent with the analytical solutions, and the accuracy is better than the RKPM.

5.2. The piezoelectric bimorph cantilever beam

The piezoelectric bimorph cantilever beam is an important component of piezoelectric devices, which can convert electrical energy to mechanical energy. In this section, a 10×1 mm^2 ($L = 10.0$ mm, $2h = 1.0$ mm) piezoelectric bimorph cantilever beam is modeled by the IRKPM and the RKPM. The piezoelectric material is PVDF, and polarized direction (P↑) and the connection between the two layers are shown in Fig. 5. The beam is assumed to be in a state of plane stress. The material properties of PVDF are listed in Table 4.

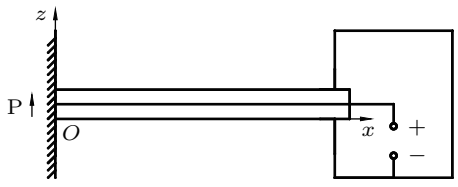


Fig. 5. The piezoelectric bimorph cantilever beam.

Table 4. The properties of PVDF.

c_{11}	2.18×10^{-3} N/μm^2	e_{31}	4.6×10^{-8} N/(V·μm)
c_{13}	6.33×10^{-4} N/μm^2	e_{33}	4.6×10^{-8} N/(V·μm)
c_{33}	2.18×10^{-3} N/μm^2	ξ^{ε}_{11}	1.062×10^{-10} N/V^2
c_{55}	7.75×10^{-4} N/μm^2	ξ^{ε}_{33}	1.062×10^{-10} N/V^2

When an external unit voltage is applied across the thickness of the piezoelectric bimorph cantilever beam, the induced strain generates to control the beam upwards bending under the effect of the electromagnetic field. The results of the analytical solutions, the proposed method, and the RKPM[6] in $z = 1.0$ mm are shown in Fig. 6 and listed in Table 5.

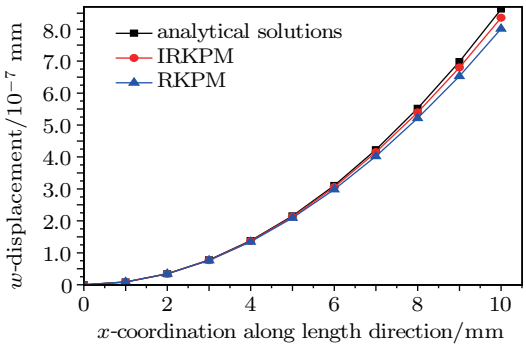


Fig. 6. (color online) The nodal displacements of the piezoelectric bimorph cantilever beam in $z = 1$ mm.

The relative errors of the IRKPM and the analytical solutions are lower than those of the RKPM[6] and the analytical solutions in $z = 1.0$ mm. The results are shown in Fig. 7 and listed in Table 5.

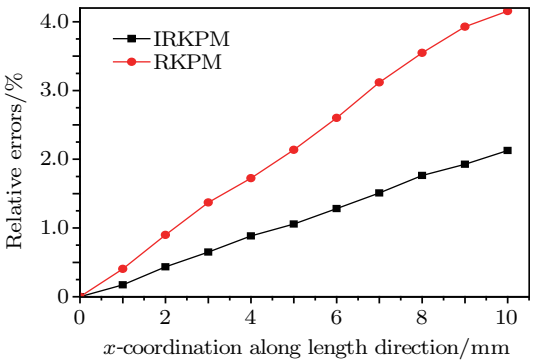


Fig. 7. (color online) Comparison of the relative errors in $z = 1.0$ mm.

Table 5. The nodal deflections and relative errors by the different methods.

Coordination	Analytical solution/mm	IRKPM displacement/mm	Relative error/%	RKPM displacement/mm	Relative error/%
(0,1)	0	0	0	0	0
(1,1)	8.6250×10^{-6}	8.6100×10^{-6}	0.17	8.5900×10^{-6}	0.41
(2,1)	3.4500×10^{-5}	3.4350×10^{-5}	0.43	3.4190×10^{-5}	0.90
(3,1)	7.7625×10^{-5}	7.7120×10^{-5}	0.65	7.6560×10^{-5}	1.37
(4,1)	1.3800×10^{-4}	1.3678×10^{-4}	0.88	1.3562×10^{-4}	1.72
(5,1)	2.1563×10^{-4}	2.1335×10^{-4}	1.06	2.1102×10^{-4}	2.14
(6,1)	3.1050×10^{-4}	3.0652×10^{-4}	1.28	3.0242×10^{-4}	2.60
(7,1)	4.2263×10^{-4}	4.1625×10^{-4}	1.51	4.0945×10^{-4}	3.12
(8,1)	5.5200×10^{-4}	5.4226×10^{-4}	1.76	5.3241×10^{-4}	3.55
(9,1)	6.9863×10^{-4}	6.8516×10^{-4}	1.93	6.7118×10^{-4}	3.93
(10,1)	8.6250×10^{-4}	8.4415×10^{-4}	2.13	8.2665×10^{-4}	4.16

Table 5 shows that the maximum relative error between the IRKPM and the analytical solutions is 2.13%, and the maximum relative error between the RKPM and the analytical solutions is 4.16%. The results obtained by using the proposed method again show close agreement with analytical solutions, and the accuracy seems better than the RKPM.

5.3. The microelectromechanical systems device

To illustrate the efficiency and accuracy of the method, the behavior of a prototype microelectromechanical systems (MEMS) device is simulated. The device is constructed by two parallel bimorphs made by PVDF and a piece of mirror, shown as Fig. 8. The properties of PVDF are given in Table 4. Both of the bimorphs are 10×1 μm, and the center of the two bimorphs is connected by a 1 μm length mirror. When the voltages are applied, the two bimorphs will deflect an adverse direction. The middle point of the mirror is changed from A to A' (as shown in Fig. 9).

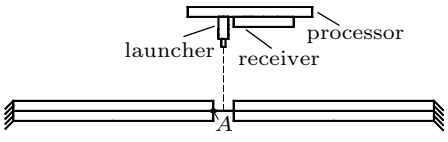


Fig. 8. The initial status of the MEMS device.

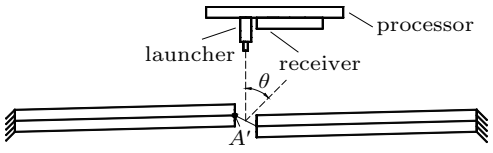


Fig. 9. The changed status of the MEMS device under different voltages.

The displacements of point A are shown in Fig. 10 and the relative errors are shown in Fig. 11. Table 6 summarizes that the maximum relative error between the measured displacement[4] and the IRKPM is 0.98%, and the maximum relative error between the measured displacement and the RKPM is 2.17%. The results obtained by the IRKPM are consistent with the measured solutions and the efficiency and accuracy is better than the RKPM.

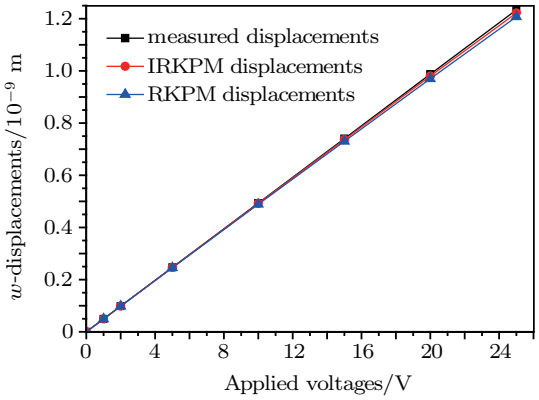


Fig. 10. (color online) The displacements of point A under different voltages.

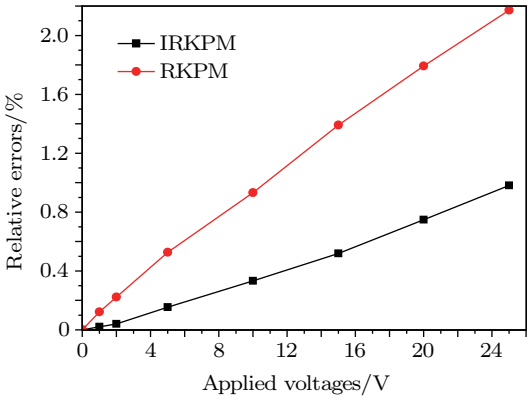


Fig. 11. (color online) The comparison of the relative errors in point A.

Table 6. Measured displacements, the displacements of the RKPM, and the IRKPM under different voltages.

Applied voltage/ V	Measured displacement/m	RKPM displacement/m	Relative error/%	IRKPM displacement/m	Relative error/%
1.00	4.936×10^{-9}	4.930×10^{-9}	0.12	4.935×10^{-9}	0.02
2.00	9.872×10^{-9}	9.850×10^{-9}	0.22	9.868×10^{-9}	0.04
5.00	2.468×10^{-8}	2.455×10^{-8}	0.53	2.4642×10^{-8}	0.15
10.00	4.936×10^{-8}	4.890×10^{-8}	0.93	4.9196×10^{-8}	0.33
15.00	7.404×10^{-8}	7.301×10^{-8}	1.39	7.3656×10^{-8}	0.52
20.00	9.872×10^{-8}	9.695×10^{-8}	1.79	9.7981×10^{-8}	0.75
25.00	1.234×10^{-7}	1.207×10^{-7}	2.17	1.22189×10^{-7}	0.98

6. Conclusion

The normal derivative of the RBF is introduced into the RKPM, and the IRKPM is proposed in this paper. This proposed method can decrease the errors on the boundary and improve the accuracy and stability of the algorithm. The IRKPM is applied to the electromechanical coupling partial differential equations of piezoelectric materials. The results obtained by the proposed method are much closer to the analytical solutions than the RKPM. Compared with the RKPM, the IRKPM has the advantages of high precision and stability on the boundary. The proposed method is a new numerical method, which has greatly developed potential.

References

[1] Zhang W, Chen L Z, Zhang J M and Huang Z G 2017 *Chin. Phys. B* **26** 048801
[2] Zhao X and Liew K M 2010 *Comput. Mech.* **45** 297
[3] Sun Y Z and Liew K M 2007 *Lecture Notes in Engineering and Computer Science* **2166** 1193
[4] Ohs R R and Aluru N R 2001 *Comput. Mech.* **27** 23
[5] Chen L, Ma H P and Cheng Y M 2013 *Chin. Phys. B* **22** 050202
[6] Cheng R J and Liew K M 2009 *Comput. Mech.* **45** 1
[7] Wang D D and Chen P J 2014 *Comput. Mech.* **54** 689
[8] Chen L, Cheng Y M and Ma H P 2015 *Comput. Mech.* **55** 591
[9] Zhang R P, Zhu J, Li X G, Loula A F D and Yu X J 2016 *Appl. Math. Model.* **40** 5096
[10] Varsamis D N and Karampetakis N P 2014 *Multidim. Syst. Sign. P* **25** 179
[11] Strozecki Y 2013 *Theory Comput. Syst.* **53** 532
[12] Mantegh I, Jenkin M R M and Goldenberg A A 2010 *J. Intell. Robot. Syst.* **59** 191
[13] Xie G Z, Zhang J M, Huang C, Lu C J and Li G Y 2014 *Comput. Mech.* **53** 575
[14] Wang J F, Sun F X and Cheng Y M 2012 *Chin. Phys. B* **21** 090204
[15] Tang Y Z and Li X L 2017 *Chin. Phys. B* **26** 030203
[16] Cheng Y M, Bai F N, Liu C and Peng M J 2016 *Int. J. Comput. Mater. Sci. Eng.* **5** 1650023
[17] Cheng Y M, Liu C, Bai F N and Peng M J 2015 *Chin. Phys. B* **24** 100202
[18] Li X L and Zhang S G 2016 *Appl. Math. Model.* **40** 2875
[19] Song C Y, Choi H Y and Lee J S 2014 *Struct. Multidisc. Optim.* **49** 851
[20] Sun F X, Wang J F, Cheng Y M and Huang A X 2015 *Appl. Numer. Math.* **98** 79
[21] Liu M B and Liu G R 2010 *Comput. Meth. Eng.* **17** 25
[22] Han Y W, Qiang H F, Liu H and Gao W R 2014 *Acta Mech. Sin.* **30** 7
[23] Congreve S and Wihler T P 2017 *J. Comput. Appl. Math.* **311** 457
[24] Liu Y, Liew K M, Hon Y C and Zhang X 2005 *Smart Mater. Struct.* **14** 1163
[25] Hon Y C, Ling L and Liew K M 2005 *Comput. Mater. Con.* **2** 39
[26] Shi J P, Ma W T and Li N 2013 *Meccanica* **48** 2263
[27] Christensen O and Massopust P 2012 *Adv. Comput. Math.* **37** 301
[28] Mirzaei D and Schaback R 2014 *Numer. Algor.* **65** 275
[29] Sheu G Y 2013 *Geotech. Geol. Eng.* **31** 1453
[30] Dai B D and Zheng B J 2013 *Appl. Math. Comput.* **219** 10044
[31] Dai B D, Cheng J and Zheng B J 2013 *Int. J. Appl. Mech.* **5** 1350011
[32] Tatari M, Kamranian M and Dehghan M 2011 *Comput. Mech.* **48** 689
[33] Huang Z Y and Yang X 2011 *J. Sci. Comput.* **49** 351
[34] Cui X Y, Liu G R and Li G Y 2011 *Arch. Appl. Mech.* **81** 1
[35] Ma J C, Wei G F, Liu D D and Liu G T 2017 *Appl. Math. Comput.* **309** 170
[36] Liu Y, Hon Y C and Liew K M 2006 *Int. J. Numer. Meth. Eng.* **66** 1153
[37] Gao H F and Wei G F 2014 *Math. Probl. Eng.* 353472
[38] Gao H F and Wei G F 2016 *Math. Probl. Eng.* **2016** 5803457
[39] Deng Y J, Liu C, Peng M J and Cheng Y M 2015 *Int. J. Appl. Mech.* **7** 1550017
[40] Cheng H, Peng M J and Cheng Y M 2017 *Eng. Anal. Bound. Elem.* **84** 52
[41] Liu W K, Jun S and Zhang Y F 1995 *Int. J. Numer. Meth. Fl.* **20** 1081
[42] Hu J Y, Sun Y and Li Q H 2016 *Chin. Phys. B* **25** 127701
[43] Wang J, Chen S S and Li Q H 2016 *Chin. Phys. B* **25** 040203